Superconducting Nanostrip Photon-Number-Resolving Detector for Photon Distribution Reconstruction

Pasquale Ercolano, Alberto Porzio, Mikkel Ejrnaes, Ciro Bruscino, Daniela Salvoni, Jia Huang, Martina Peluso, Chengjun Zhang, Hao Li, Lixing You, Loredana Parlato, and Giovanni Piero Pepe

(Invited Paper)

***Abstract*—Single photon detectors based on superconducting nanostrips demonstrated high performance at 1550 nm, combining high efficiency and low noise. Arranged in arrays, these devices can implement photon-number resolution, expanding the range of applicability of superconducting detectors. A detector of this kind was used in our recent work to implement the annihilation operator and the characterization of quantum states in terms of their photon number distribution. The reconstructed distributions were consistent with the theoretical predictions, exhibiting fidelities higher than 99.9%. In this work, this procedure was repeated with each pixel singularly to define a detector fidelity matrix, evaluating the fidelity among all the possible pixel combinations. In this way, we introduce an additional tool that quantifies not only the quality of the reconstructed photon number distribution when compared to the theoretical expectation, but also the mutual fidelity when different pixels are chosen as independent, and then the fabrication uniformity.**

***Index Terms*—Infrared detectors, nanowire single-photon detectors, superconducting detectors.**

I. Introduction

A DETECTOR able to resolve the number of photons is crucial for a wide range of applications, including quantum key distribution [1], linear optics quantum computing [2], quantum random number generation [3], photon sources and detectors calibration [4]. However, many applications rely on photons at telecom wavelengths, where conventional semiconductor-based detectors are outperformed by superconducting nanostrip single photon detectors (SNSPDs). Indeed, SNSPDs offer an excellent alternative, combining high detection efficiency at 1550 nm with a low dark count rate (DCR) [5]. In addition, arranged in arrays, these detectors proved to be able to resolve the number of incoming photons [6]. This feature is highly relevant in n-photon state quantum optics experiments, including photon state engineering and its subsequent characterization [7], [8], [9]. In particular, SNSPDs have been already employed in implementing the annihilation operator at telecom wavelength [10]. Quantum state reconstruction is typically achieved by homodyne detection, but this requires a complex setup when a pulsed source is employed [11]. Conversely, superconducting nanostrip photon-number-resolving detectors (PNRDs) can efficiently reconstruct photon number distributions at telecom wavelength, resulting in a valuable tool in experiments where this information is crucial [12].

In this work, we present measurements performed with an eight-pixel superconducting nanostrip PNRD composed of independently biased NbN nanostrips. Thanks to the interleaved geometry, the incoming light is uniformly distributed over them. In our approach, introduced in [12], we implement both photon subtraction and characterization of the resulting state by means of a single PNRD. This is possible by subtracting a photon with a single pixel and using the others for the reconstruction. Then, the statistical analysis of the measured detection events, as well as the knowledge of the response matrix, allows us to reconstruct photon number distributions with high fidelity. In addition to our previous work [12], by changing the independent pixel for subtraction every time, in this work we define a fidelity matrix, which represents a quantitative method to test the outcome of the fabrication of a PNRD in terms of uniformity of the pixels.

II. Theoretical Model

Photon subtraction can be achieved by a low-reflectivity beam splitter [13]. In order to show it, we take into account the diagonal

Received 12 October 2025; revised 21 January 2026; accepted 10 February 2026. Date of publication 10 March 2026; date of current version 23 March 2026. This work was supported in part by "Quantum Italy Deployment (QUID)" under Project 101091408 (Digital Europe Programme), in part by "SMIRNe" Project (FRA - Programma per il Finanziamento della Ricerca di Ateneo 2024 Tip. under Grant A CUP E63C24002560005), and in part by the "Innovation Program for Quantum Science and Technology" under Grant 2023ZD0300100. *(Corresponding author: Pasquale Ercolano.)*

Pasquale Ercolano, Ciro Bruscino, Martina Peluso, Loredana Parlato, and Giovanni Piero Pepe are with the Dip. di Fisica "E. Pancini", Università degli Studi di Napoli Federico II, I-80125 Napoli, Italy (e-mail: pasquale.ercolano@unina.it).

Alberto Porzio is with the DICEM Università di Cassino e del Lazio Meridionale, 03043 Cassino, Italy.

Mikkel Ejrnaes is with the CNR-SPIN Institute of Superconductors, Innovative Materials and Devices, 80078 Pozzuoli, Italy, and also with Qunatech SRL, 80128 Napoli, Italy.

Daniela Salvoni and Chengjun Zhang are with Qunatech SRL, 80128 Napoli, Italy, and also with Photon Technology Italy SRL, 80128 Napoli, Italy.

Jia Huang, Hao Li, and Lixing You are with the Shanghai Key Laboratory of Superconductor Integrated Circuit Technology, Shanghai Institute of Microsystem and Information Technology, Chinese Academy of Sciences, Shanghai 200050, China.

Color versions of one or more figures in this article are available at https://doi.org/10.1109/TASC.2026.3672096.

Digital Object Identifier 10.1109/TASC.2026.3672096

elements of a generic state density matrix in the Fock representation. The other terms are not relevant for the characterization in terms of the photon number, which is our goal. The initial density matrix diagonal is:

$$\hat{\rho} = \sum_{n=0}^{\infty} \rho_n \, |n\rangle \langle n| \, . \tag{1}$$

When it enters the beam splitter, with transmissivity T and reflectivity R, it becomes:

$$\hat{\rho}_{ab} = \sum_{n=0}^{\infty} \sum_{k=0}^{n} (nk) \, \rho_n T^{n-k} R^k \, |n-k\rangle_a \, |k\rangle_b \, \langle k|_a \, \langle n-k| \, , \tag{2}$$

where the subscript a indicates the transmission port and b the reflection one. In order to get the state on mode a heralded by a photon detection on mode b, we employ a positive operator-valued measure (POVM):

$$\widehat{\prod}_1 = \sum_{i=0}^{\infty} \sigma_{1i} \, |i\rangle \langle i| \, , \tag{3}$$

where σ is the response matrix of the detector on mode b. In the case of an SNSPD, it is the probability of recording one detection event when i photons arrive:

$$\sigma_{1i} = 1 - (1-\eta)^i. \tag{4}$$

Then, the heralded state on mode a after single photon detection on mode b is:

$$\hat{\rho}'_a = \frac{Tr_b \left(\hat{\rho}_{ab} \widehat{\prod}_1 \right)}{Tr \left(\hat{\rho}_{ab} \widehat{\prod}_1 \right)}, \tag{5}$$

where Tr_b refers to the partial trace on mode b. Since $R \ll 1$, we approximate to the first order in R. In addition, since $T \approx 1$, we also approximate T^{n-1} with 1 for any n. Finally, since $\sigma_{10} = 0$, the first term is with $k = 1$. Under these assumptions, we get:

$$Tr_b \left(\hat{\rho}_{ab} \widehat{\prod}_1 \right) = \sigma_{11} R \sum_{n=0}^{\infty} (n+1) \; \rho_{n+1} \; |n\rangle_a \langle n| \, . \tag{6}$$

Hence, the resulting diagonal of the conditioned state is:

$$\hat{\rho}' = \frac{\sum_{n=0}^{\infty} (n+1) \; \rho_{n+1} \; |n\rangle \langle n|}{\sum_{i=0}^{\infty} (i+1) \; \rho_{i+1}}. \tag{7}$$

This corresponds to the state that we get when we apply the annihilation operator:

$$\hat{\rho}' = \frac{\hat{a} \, \hat{\rho} \, \hat{a}^\dagger}{Tr \left(\hat{a} \, \hat{\rho} \, \hat{a}^\dagger \right)}. \tag{8}$$

We describe how the PNRD acts on the state on mode a, represented now by a generic $\hat{\rho}$. In order to get the detection event distribution, we use again a POVM. Therefore, the probability of recording m detection events is:

$$P_m = Tr \left(\hat{\rho} \widehat{\prod}_m \right). \tag{9}$$

Here, the elements σ_{vi} of the response matrix of an N-pixel PNRD, corresponding to the probability of recording v detection events when i photons arrive, can be written as [14]:

$$\sigma_{vi} = \binom{N}{v} \sum_{j=0}^{v} (-1)^j \binom{v}{j} \left[(1-\eta) + \frac{v-j}{N} \eta \right]^i. \tag{10}$$

In order to retrieve the probabilities ρ_n from P_m, we employ the expectation-maximization-entropy (EME) method by Hloušek et al. [15]. It is an iterative method, with initialization condition:

$$\rho_n^{(0)} = \frac{1}{n_{max}+1}, \tag{11}$$

where n_{max} is the number of terms of the reconstructed distribution. In particular, we need n_{max} higher than the average number of photons μ. The term $\rho_n^{(k)}$ of the photon number distribution, at the iteration step (k) of the algorithm, is calculated as:

$$\rho_n^{(k+1)} = \prod_n^{(k)} \rho_n^{(k)} - \lambda \left(\ln \rho_n^{(k)} - S^{(k)} \right) \rho_n^{(k)}. \tag{12}$$

Here, λ is a scale factor chosen equal to 10^{-3} as in [15]. Finally, the quantities $\prod_n^{(k)}$ and $S^{(k)}$ are:

$$\prod_n^{(k)} = \sum_m \frac{P_m \, \sigma_{mn}}{\sum_j \sigma_{mj} \, \rho_j^{(k)}}, \tag{13}$$

$$S^{(k)} = \sum_n \rho_n^{(k)} \ln \rho_n^{(k)}. \tag{14}$$

In order to quantify the comparison between the reconstructed photon distribution and its theoretical expectation, we introduce the fidelity:

$$F = \left(\sum_n \sqrt{\rho_n^{reconstructed} \rho_n^{theoretical}} \right)^2. \tag{15}$$

III. Experimental Setup

The experimental setup is based on a Gifford-McMahon cryocooler, working at a temperature of 2.2 K. Our detector is a PNRD based on an array of eight superconducting NbN nanostrips, whose thickness is 6 nm. The width of each nanostrip is 75 nm, with a pitch of 180 nm, resulting in an active area of diameter 15 μm. The fiber, mounted on the chip holder, was coupled through an infrared camera at room temperature, optimizing the coupling efficiency. The light source is a fiber-coupled pulsed laser at 1550 nm, whose repetition rate is 20 MHz. A rotating disk can be placed to modify the photon distribution from Poissonian to Thermal [16]. The mean photon number per pulse can be modified by a variable optical attenuator. The polarization is aligned by a three-paddle polarization controller. The detector is connected to a readout and bias electronic module. Its output, together with the laser trigger, is recorded by a time-to-digital converter. A scheme of the experimental setup is shown in Fig. 1.

IV. Results

Preliminarily to the photon-subtraction measurements, each pixel of the superconducting nanostrip PNRD, considered as an independent detector, has been characterized in terms of its detection efficiency and DCR. This operation was carried out

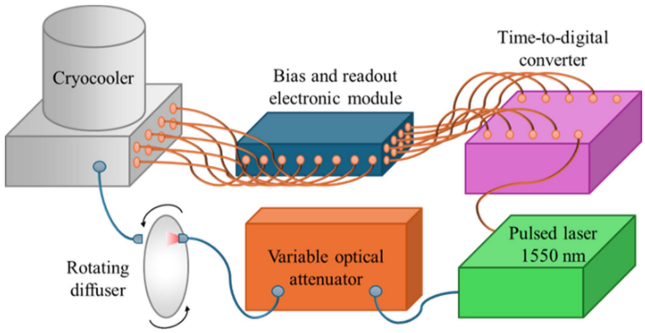

Fig. 1. Scheme of the experimental setup. The photon distribution from a pulsed laser can be modified from Poissonian to Thermal by means of a rotating disk.

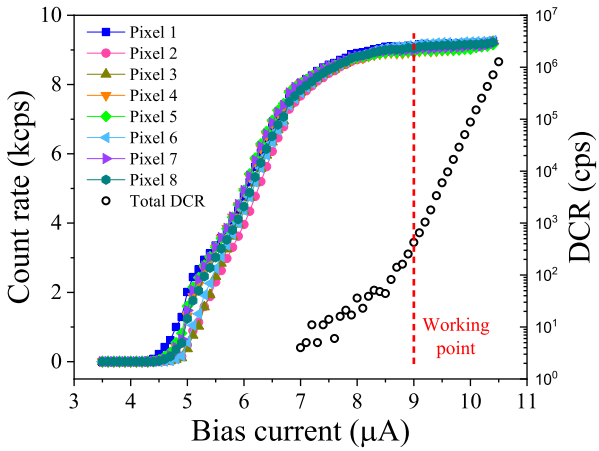

Fig. 2. Count rate contribution from each pixel and total DCR, as a function of the bias current, with an input photon rate of 100 kHz. The dashed red line indicates the working point.

by measuring the photon rate entering the cryocooler from the fiber outside. This was possible by means of a calibrated power meter. In Fig. 2, we report the count rate, measured with an input photon rate of 100 kHz, as a function of the bias current. We note that each pixel provides a value consistent with the others. The working point was chosen as the bias current at which the DCR is 100 cps. The detection efficiency is evaluated as the count rate divided by the input photon rate, resulting in 72% for the entire PNRD. We also measured the recovery time of the nanostrips, obtaining 6 ns [17].

The annihilation operator is implemented considering an independent pixel. Indeed, thanks to the interleaved geometry, the light is equally divided among the nanostrips. In this configuration, we have a beam splitter with transmissivity 87.5%, dividing the light between an SNSPD (the independent pixel) and a seven-pixel PNRD (Fig. 3). Therefore, we can refer to the theoretical framework described in Section II. We use the independent pixel to perform photon subtraction and the other to reconstruct the photon number distribution, both with and without applying the annihilation operator.

We now discuss the results obtained when the first pixel (Fig. 3) is considered independent. Fig. 4 reports the normalized detection event distribution. This is acquired by counting the number of times in which, in correspondence of a laser pulse,

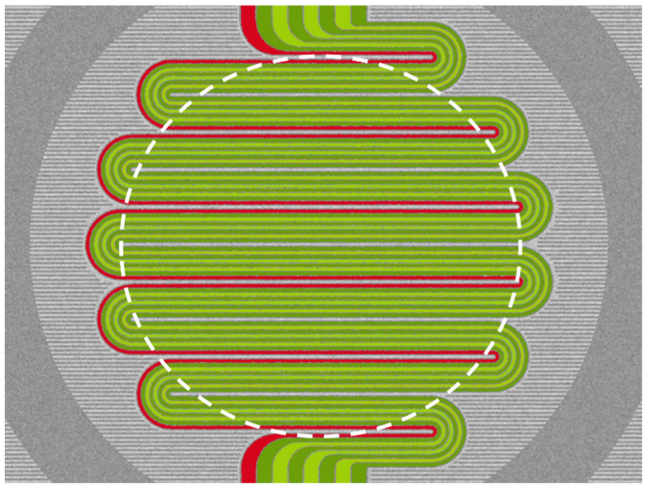

Fig. 3. Subdivision of the superconducting nanostrip PNRD: the independent pixel used for subtraction is colored red, the pixel used for reconstruction are colored green. The dashed white circle highlights the area illuminated by the fiber.

TABLE I
MEAN PHOTON NUMBER PER PULSE AND FIDELITY OF THE PHOTON NUMBER DISTRIBUTIONS, WITH AND WITHOUT DISK, WITH AND WITHOUT APPLYING THE ANNIHILATION OPERATOR

	Original		Photon subtracted	
	μ	F (%)	μ'	F' (%)
Without disk	1.33+0.01	99.997±0.002	1.33+0.01	99.995±0.002
Rotating disk	0.73+0.01	99.985±0.002	1.43+0.01	99.90±0.01

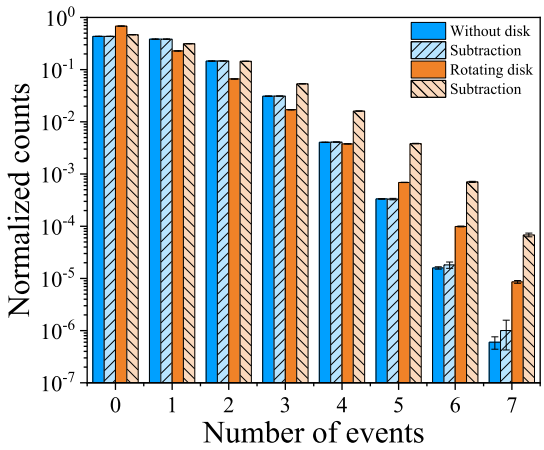

Fig. 4. Normalized detection event distribution. In the case without disk, the original distribution is colored blue and the photon-subtracted one is colored light blue. In the case with rotating disk, the original distribution is colored orange and the photon-subtracted one is colored light orange.

a certain number of nanostrips of the seven-pixel PNRD have switched. In order to study how this is modified by the annihilation operator, we also acquired the same quantity only in the case in which the first pixel switched. This measurement was performed both with Poissonian (without disk) and Thermal

TABLE II
FIDELITY MATRIX WITHOUT DISK AND WITHOUT APPLYING THE ANNIHILATION OPERATOR

99.997±0.002	99.989±0.009	99.987±0.009	99.989±0.009	99.992±0.008	99.992±0.008	99.989±0.009	99.985±0.009
99.984±0.009	99.997±0.002	99.990±0.009	99.994±0.006	99.996±0.004	99.995±0.005	99.993±0.007	99.981±0.009
99.994±0.004	99.989±0.009	99.998±0.002	99.990±0.009	99.987±0.009	99.986±0.009	99.992±0.008	99.991±0.006
99.988±0.009	99.991±0.009	99.995±0.005	99.997±0.002	99.986±0.009	99.992±0.007	99.995±0.005	99.990±0.009
99.995±0.004	99.995±0.004	99.993±0.007	99.985±0.009	99.998±0.002	99.996±0.003	99.994±0.006	99.995±0.004
99.991±0.009	99.994±0.006	99.990±0.009	99.995±0.005	99.994±0.003	99.998±0.002	99.991±0.008	99.995±0.003
99.995±0.005	99.990±0.009	99.997±0.002	99.994±0.006	99.995±0.005	99.997±0.002	99.997±0.002	99.994±0.004
99.984±0.009	99.992±0.007	99.992±0.007	99.985±0.009	99.987±0.009	99.996±0.004	99.987±0.009	99.997±0.002

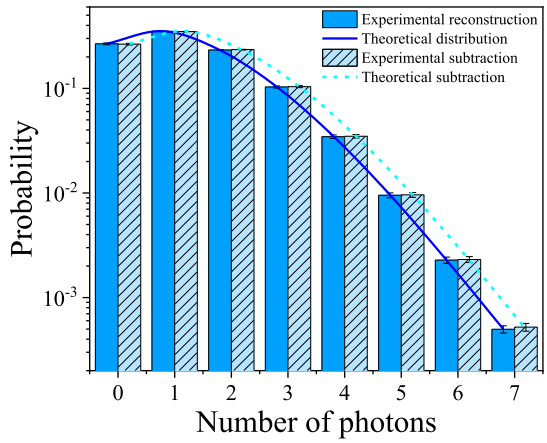

Fig. 5. Photon number distributions in the case without disk. The original distribution reconstructed by data is colored blue, and its theoretical expectation is the blue solid curve. The photon-subtracted distribution reconstructed by data is colored light blue, and its theoretical expectation is the light blue dashed curve.

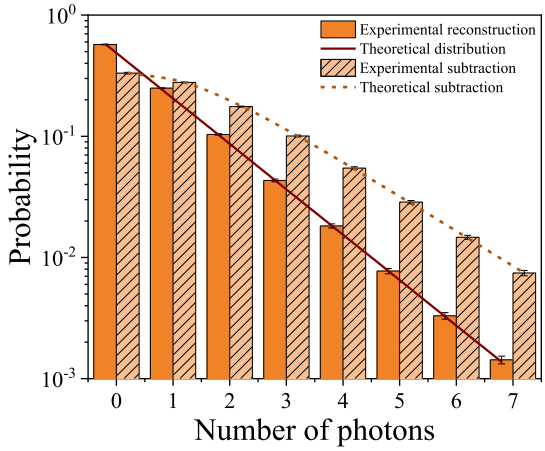

Fig. 6. Photon number distributions in the case with rotating disk. The original distribution reconstructed by data is colored orange, and its theoretical expectation is the brown solid curve. The photon-subtracted distribution reconstructed by data is colored light orange, and its theoretical expectation is the light brown dashed curve.

(rotating disk) photon number distributions. Fig. 4 reports our experimental data. We note that the normalized counts without disk, applying and not applying the subtraction, are consistent within the errors. Conversely, the normalized counts with rotating disk, applying and not applying the subtraction, are sensitively different. This is in agreement with our expectations [13]: the coherent state (Poissonian distribution) is eigenstate of the annihilation operator, and then it has to remain the same. Conversely, when the annihilation operator is applied on a thermal state, its mean number of photons doubles.

These normalized counts are an estimation of the probabilities P_m, which, together with the response matrix, allow us to use the EME method in order to reconstruct the photon number distribution. Since we work with $\mu \sim 1$ and the repetition rate of the laser is 20 MHz, the DCR is much smaller and then can be neglected in the reconstruction algorithm.

Figs. 5 and 6 show our results. The photon number distributions reconstructed from our experimental data are consistent with the theoretical expectations, both with and without disk, both with and without the application of the annihilation operator. Table I reports the mean photon number, showing that, after photon subtraction, it remains the same without disk (coherent state), but it doubles with rotating disk (thermal state). In order to quantify the agreement with the theoretical distribution, the fidelity is evaluated, too. It is near unit, demonstrating that we succeeded in reconstructing each photon distribution.

Since the pixels are equivalent, this procedure can be repeated by choosing each pixel as independent. In the case of sufficient uniformity among the pixels, the reconstructed distributions are not only consistent with the theoretical expectations, but also with the ones obtained with different independent pixels.

We summarized this comparison by introducing a fidelity matrix F_{ij},. The out-diagonal elements ($i \neq j$) represent the fidelity between the distribution reconstructed using pixel i as independent and the one using pixel j as independent. Conversely, the diagonal elements ($i = j$) indicate the fidelity between the distribution reconstructed using pixel i as independent and the expected theoretical distribution.

In this way, we obtained fidelity values greater than 99.9% in any configuration, demonstrating both the efficiency of this method for reconstructing the photon number distribution, also after photon subtraction, and the accuracy of the fabrication process, which ensured uniformity among the nanostrips of the array.

As example, we show in Table II the fidelity matrix corresponding to the measurement without disk and without applying the annihilation operator.

V. Conclusion

Superconducting nanostrip PNRDs are tools suitable for experimental applications which require photon-number resolution with the high efficiency and low dark count rate characteristic of the SNSPDs. The interleaved geometry, in particular, ensures that the light is equally divided among the pixels composing the detector. This allows for a straightforward description of its response in terms of a matrix and the reconstruction of photon number distributions through the EME method.

In this work, we used the independence of the pixels to implement, within a single PNRD, both photon subtraction and quantum state characterization. We demonstrated, by changing the independent pixel time by time, that our PNRD exhibits a high uniformity among its superconducting nanostrips. In order to provide a representation of this feature through a clear and quantitative methodology, we introduced a fidelity matrix as a dedicated metric for assessing PNRD uniformity, obtaining values exceeding 99.9% across all our pixels.

References

[1] W. Lei et al., "High-rate quantum key distribution exceeding 110 Mb s^{-1}," *Nature Photon.*, vol. 17, no. 5, pp. 416–421, Mar. 2023.

[2] E. Knill, R. Laflamme, and G. J. Milburn, "A scheme for efficient quantum computation with linear optics," *Nature*, vol. 409, pp. 46–52, Jan. 2001.

[3] P. Ercolano et al., "Superconducting nanostrip photon-number-resolving detector as an unbiased random number generator," *IEEE Trans. Quantum Eng.*, vol. 5, Jul. 2024, Art. no. 4100808.

[4] A. L. Migdall, D. Branning, and S. Castelletto, "Tailoring single-photon and multiphoton probabilities of a single-photon on-demand source," *Phys. Rev. A*, vol. 66, no. 5, Nov. 2022, Art. no. 053805.

[5] L. You, "Superconducting nanowire single-photon detectors for quantum information," *Nanophotonics*, vol. 9, no. 9, pp. 2673–2692, Jun. 2020.

[6] P. Ercolano et al., "Time binning method for nonpulsed sources characterization with a superconducting photon number resolving detector," *IEEE Trans. Quantum Eng.*, vol. 4, Sep. 2023, Art. no. 4100609.

[7] A. Divochiy et al., "Superconducting nanowire photon number resolving detector at telecom wavelength," *Nature Photon.*, vol. 2, pp. 302–306, Apr. 2008.

[8] N. Biagi, S. Francesconi, A. Zavatta, and M. Bellini, "Photon-by-photon quantum light state engineering," *Prog. Quantum Electron.*, vol. 84, Jun. 2022, Art. no. 100414.

[9] C. Bruscino et al., "Reduction of $g^2(0)$ value in heralded spontaneous parametric down-conversion sources using photon number resolving detectors," *Low Temp. Phys.*, vol. 50, pp. 24–28, Jan. 2024.

[10] M. F. Melalkia et al., "Plug-and-play generation of non-Gaussian states of light at a telecom wavelength," *Opt. Exp.*, vol. 30, no. 25, pp. 45195–45201, Dec. 2022.

[11] M. Endo et al., "Non-Gaussian quantum state generation by multi-photon subtraction at the telecommunication wavelength," *Opt. Exp.*, vol. 31, no. 8, pp. 12865–12879, Apr. 2023.

[12] P. Ercolano et al., "Photon statistics of one-and two-photon subtracted states at telecom wavelength reconstructed via direct detection," *Opt. Exp.*, vol. 33, no. 16, pp. 33446–33455, Jul. 2025.

[13] V. Parigi, A. Zavatta, M. Kim, and M. Bellini, "Probing quantum commutation rules by addition and subtraction of single photons to/from a light field," *Science*, vol. 317, no. 5846, pp. 1890–1893, Sep. 2007.

[14] M. J. Fitch, B. C. Jacobs, T. B. Pittman, and J. D. Franson, "Photon-number resolution using time-multiplexed single-photon detectors," *Phys. Rev. A*, vol. 68, no. 4, Oct. 2003, Art. no. 043814.

[15] J. Hloušek, M. Dudka, I. Straka, and M. Ježek, "Accurate detection of arbitrary photon statistics," *Phys. Rev. Lett.*, vol. 123, no. 15, Oct. 2019, Art. no. 153604.

[16] F. T. Arecchi, "Measurement of the statistical distribution of Gaussian and laser sources," *Phys. Rev. Lett.*, vol. 15, no. 24, Dec. 1965, Art. no. 912.

[17] P. Ercolano et al., "Superconducting PNR detector for photon sources characterization," *IEEE Trans. Appl. Supercond.*, vol. 34, no. 3, May 2024, Art. no. 2200105.